Review Article

Christian Brütting, Tobias Standau, Johannes Meuchelböck, Peter Schreier, and Holger Ruckdäschel*

A review on semi-crystalline polymer bead foams from stirring autoclave: Processing and properties

https://doi.org/10.1515/epoly-2023-0092
received July 05, 2023; accepted August 09, 2023

Abstract: Bead foams have been widely used for more than 70 years, with expandable polystyrene and expanded polypropylene (EPP) being the main materials. There are different processes for producing bead foams, depending heavily on the material used (e.g., their thermal behavior). EPP is usually produced by a discontinuous stirring autoclave process, which is the main subject of this study. In this process, thermal treatment during the saturation phase leads to the formation of a second melt peak, which is considered an important prerequisite for the subsequent welding process, in which the individual foamed beads are welded into complex shaped parts by applying saturated steam to the beads in a cavity (so-called steam chest molding). To date, EPP is one of the main bead foams used industrially, but other materials such as polylactide and thermoplastic polyurethane can also be processed using the same technique. This review focuses on the important thermal and physical mechanisms during saturation and expansion and the parameters (material and process) that affect them. The process itself provides multiple possibilities to influence thermal behavior (i.e., crystallization) and expansion. Typical properties of resulting bead foams, which are found in many applications, are also considered.

*** Corresponding author: Holger Ruckdäschel,** Department of Polymer Engineering, University of Bayreuth, Universitätsstraße 30, 95447 Bayreuth, Germany; Neue Materialien Bayreuth GmbH, Gottlieb-Keim-Straße 60, 95448 Bayreuth, Germany; Bavarian Polymer Institute and Bayreuth Institute of Macromolecular Research, University of Bayreuth, Universitätsstraße 30, 95447 Bayreuth, Germany, e-mail: holger.ruckdaeschel@uni-bayreuth.de
Christian Brütting, Tobias Standau, Johannes Meuchelböck: Department of Polymer Engineering, University of Bayreuth, Universitätsstraße 30, 95447 Bayreuth, Germany
Peter Schreier: Neue Materialien Bayreuth GmbH, Gottlieb-Keim-Straße 60, 95448 Bayreuth, Germany

Keywords: bead foams, stirring autoclave, mechanical properties, expanded polypropylene, expanded polylactide

1 Introduction

Bead foams (also, but less commonly, called particle foams) were invented in the middle of the last century. In 1949, the first bead foam made of polystyrene was patented by BASF (1). In the 1970s/80s, bead foams made of polyolefins (i.e., polyethylene [PE] and polypropylene [PP]) were established in the market (2,3). The evolution of bead foams was summarized in a previous paper (4); it is worth noting that there have been many innovations in the last two decades. Some studies have been carried out to broaden the field of applications of bead foams by using other polymers with higher performance (4).

To date, the bead foam with the highest market share is still expandable polystyrene (EPS). In 2022, global EPS consumption was around 7.2 million tons. Overall, the Asia-Pacific region is consuming the most EPS: around 57% of global EPS consumption in 2022 (5). The global EPS market is anticipated to grow at a compound annual growth rate (CAGR) of 5% (6).

Here, in principle, polystyrene microgranules can be impregnated with an organic blowing agent (usually pentane) during suspension polymerization to produce expandable beads (i.e., EPS). Foaming is then initiated in a separate step, usually by exposing these impregnated microgranules to hot steam (so-called pre-foaming). The final step is welding the beads into a final part in a cavity, which is also typically done with hot steam in a steam chest molding (SCM) machine. It is worth noting that a process like EPS production for obtaining EPP beads only works for amorphous polymers with a T_g above the room temperature and could not yet be established for semi-crystalline polymers such as PP as the gas sorption and storage are hindered by the crystalline phase and its T_g is below room temperature, which leads to

higher pentane diffusion. In consequence, gas storage and shelf life would be unfavorable.

Unlike EPS, the second most important bead foam – EPP – is foamed in significant quantities in a discontinuous autoclave process. Although it is possible to obtain EPP in a continuous process (i.e., in a foam extruder coupled with an underwater pelletizer) (7).

Autoclave foaming is commonly used in academia as a screening method and several methods have been established, such as temperature and pressure-induced foaming, respectively. Besides these lab-scale methods with small devices that are mainly interesting from a scientific point of view, EPP is industrially produced in larger vessels with water as a heat transfer media and stirrer. Here, the main difference from other autoclave processes is scalability. A large volume of pellets can be processed in a stirred autoclave, while a standard autoclave system without water would lead to fusion of the particles in the pressure chamber. Therefore, the stirred autoclave can produce larger volumes of particles and is therefore of greater importance to the industry. The reason for using the stirring autoclave is based on the induced thermal characteristics of the beads, which are considered an important prerequisite for the following welding of these beads in the SCM process. As summarized in Figure 1, the process chain for the production of EPP starts with (i) the production of small spherical granules (so-called µ-granules with a diameter of around 1 mm) from the polymer including additives, (ii) followed by autoclave foaming of the µ-granules, and is completed (iii) by welding, where the foamed beads are welded (*via* steam) to a final part with SCM.

Main manufacturers of EPP are JSP Corp. (Japan, brand name: Arpro), Kaneka Corp. (Japan, brand name: Eperan™), and BASF SE (Germany, brand name: Neopolen®). Europe, the Middle East, and Asia consume a total of about 40,000 tons of EPP, while global consumption reaches 170,000 tons (8). The EPP production is anticipated to expand at a CAGR of around 1% from 2023 to 2030 (9). About two-thirds are used in automotive applications, such as sun visors, bumper cores, or covers (10). Other typical applications are higher quality multiple use packaging, insulation boxes, furniture, and health, ventilation, and air conditioning applications. The stirring autoclave process is mainly used for the production of EPP (11–13) or thermoplastic polyurethane (ETPU) (14). In addition, the production of foamed beads in a stirring autoclave has been described in the literature for PLA (15,16), PC (17), LDPE (18), PEBA (19), as well as blends of PP and PLA (20).

In Table 1, some important properties of the bead foams that are established in the market are summarized. So far, only a few bead foams could be established. Besides EPS and EPP, based on commodity polymers, ETPU is used due to its elastomeric properties. A comparison of commercial bead foams is quite complicated since they have very different properties. EPS as an example with its high T_g at about 100°C is very rigid, while EPP is quite soft. On the other side, ETPU is completely different in its behavior due to its highly elastic behavior. In general, this can be seen in the elongation at break (note: the densities are different here). Here EPS shows the lowest and ETPU the highest elongation at break, indicating that ETPU is more elastic compared to EPS. Other properties such as compression stress or thermal conductivity are highly affected by density and cell size and additives.

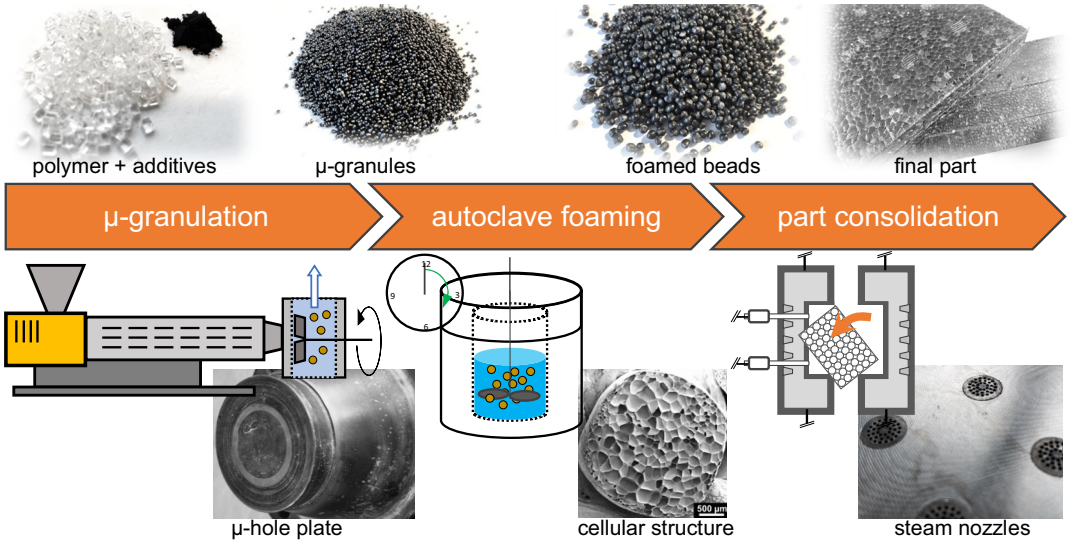

Figure 1: Overview of the process chain of bead foam production with a stirring autoclave. Copyright © 2023; University of Bayreuth, Department of Polymer Engineering.

Table 1: Selected properties of EPS, EPP, and E-TPU

Property	EPS (70 kg·m^{-3})	EPP (60 kg·m^{-3})	ETPU (250 kg·m^{-3})
Tensile strength (kPa)	100	880	600
Elongation at break (%) (tensile)	1–2 (30 kg·m^{-3} (21))	27	125
Compression stress at 10%, 25%, 50% compression (kPa)	70, –, –	310, 370, 550	55, 130, 275
Residual compressive strain (50%, 22 h, 23°C) 24 h after relaxation (%)	—	26	<5
Thermal conductivity (W·m^{-1}·K^{-1})	0.032	0.04	—
Chemical resistance	Very low	Very high	Very high
Reference	(21,22)	(23)	(24)

This review provides an overview about the processing of bead foams *via* the stirring autoclave route and analyzes the work which has been done in this field – to identify potential research fields and future trends.

2 Processing of expanded bead foams

2.1 Production of µ-granules

The µ-granules can be produced in a continuous extrusion process. For this purpose, the polymer and all required additives (e.g., pigments) are mixed and extruded through a die plate and cut by an underwater granulator (UWG). Since the die plate consists of several holes with small diameter, so-called µ-granules can be obtained. Typical particle sizes for these microparticles are less than 1 mm. The small diameter can be considered advantageous (i) for subsequent sorption in the autoclave, allowing a shorter saturation time, and (ii) to obtain smaller foamed beads that can be used to realize a smaller wall thickness in the molded part. However, the processing is not trivial as the small holes can be easily plugged. In addition, non-spherical µ-granules may result from inappropriate rheological behavior and the ductile PP tends to form tails. Figure 2 shows µ-granules of different appearances.

2.2 Bead foaming in stirring autoclave process

For the production of EPP, the material is usually composed of random copolymers of PP (with PE or polybutylene [PB]) with different rheological properties (25,26).

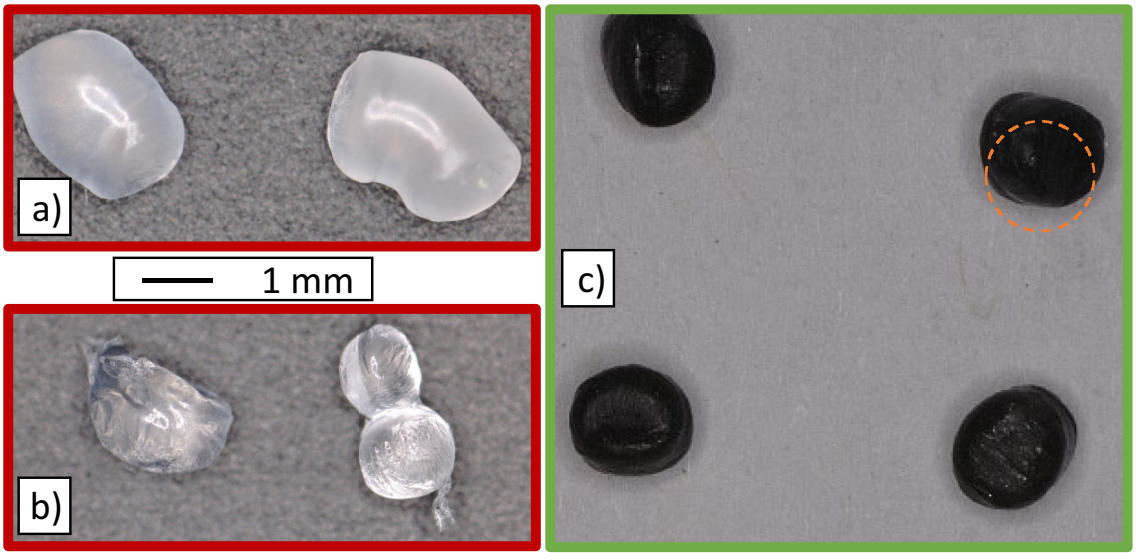

Figure 2: Appearance of µ-granules: (a) non-spherical shape because of insufficient melt flow behavior, (b) tails and agglomeration from insufficient cutting by the UWG, and (c) optimum spherical shape of µ-granules. Copyright © 2023; University of Bayreuth, Department of Polymer Engineering.

Carbon black is often used as a pigment and nucleating agent, as described in patents (27). The materials are usually processed in a stirring autoclave. The general foaming setup is shown in Figure 3. Here, the polymer is dispersed in water and dispersants (25,26,28), and a blowing agent (usually CO_2 (25,26), N_2, and/or butane (28)) is injected. The system is treated at elevated temperatures, i.e., usually near the melting point. The suspension is mixed with a rotor blade (stirrer) in the autoclave to ensure good heat exchange. In the following, the theoretical background regarding the sorption during the process is first provided. Afterwards, the process and its dependence on the processing parameters are described.

2.2.1 Theoretical background

During this saturation step, the blowing agent is absorbed by the µ-granules. However, the crystalline structure of the µ-granules changes during this thermal treatment.

The special thermal treatment can result in the formation of two melting peaks during the saturation phase, which are beneficial for subsequent bead fusion (i.e., welding). The formation of these two melting peaks is a very complex process depending on various process parameters (blowing agent, pressure, temperature) that influence the crystal rearrangement. After the saturation step, a depressurization valve is opened, and the suspension is flushed out of the autoclave. This rapid pressure drop initiates the foaming process of the µ-granules. Any change in suspension of the materials, in saturation conditions, and in depressurization affects the morphological and thermal properties. The influence of the process parameters on these properties will be described later. First, the basic principle of generating two separate melting peaks will be described.

The µ-granules used are usually semi-crystalline polymers that have a defined melting range. This melting range is characterized by the onset, offset, and melting peak (T_{m0}). During the autoclave process, the entire system is heated to a temperature close to the melting peak (i.e., between onset and offset). The saturation phase leads to the plasticization and reorganization of the crystal lamellas and is schematically proposed in Figure 4. Due to plasticization by the blowing agent, the crystals melt at a lower

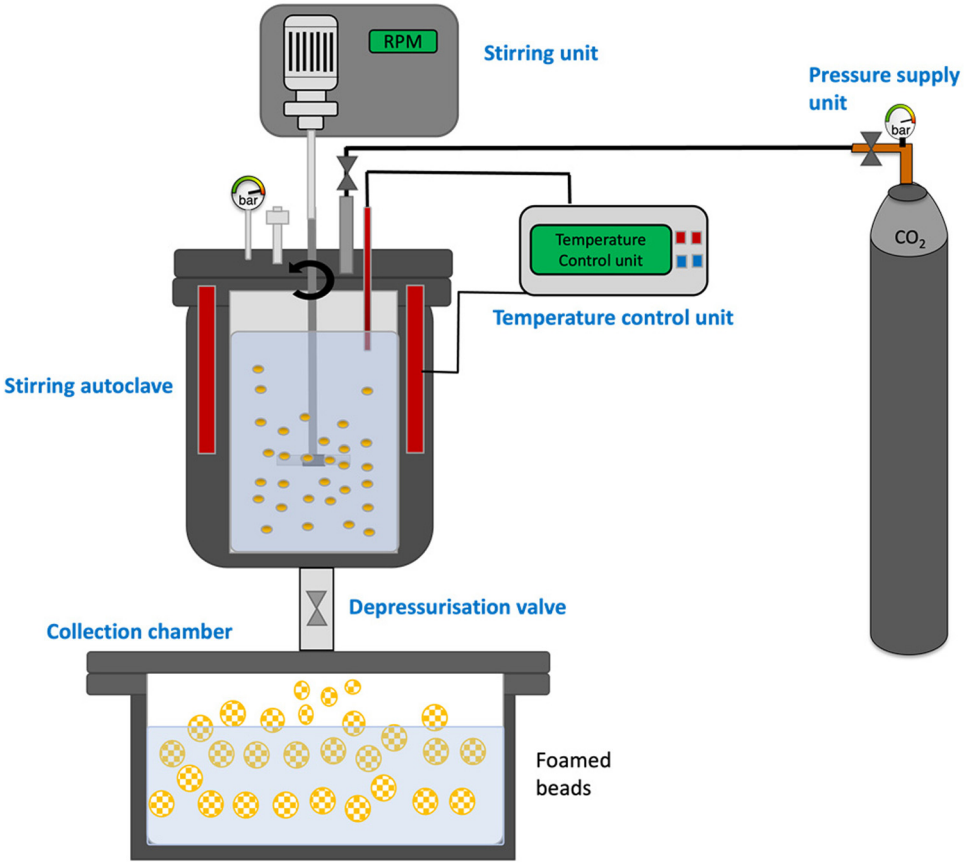

Figure 3: Laboratory-scale set-up for bead foam production *via* stirring autoclave. Copyright © 2023; University of Bayreuth, Department of Polymer Engineering.

temperature as the chain mobility increases. This increased mobility is also known to reduce the glass transition (29–31).

During the saturation process, the unmolten crystals undergo a perfection process that leads to an increase in lamellar thickness (i.e., a more ordered crystal structure). This increase in lamellar thickness increases the melting range of the unmolten crystals and leads to a second melting peak at higher temperatures ($T_{m,2}$). This phenomenon was described without the presence of CO_2 by Hingman et al. (32). After the saturation process, the system is depressurized. This step leads to foaming and the beads are purged into a collection vessel where they are cooled and stabilized. The foaming and cooling process leads to recrystallization of the molten crystals. This recrystallized phase forms itself usually in a similar temperature range ($T_{m,1}$) slightly below the original melting range ($T_{m,0}$). This change in melting range is shown for unprocessed PP and foamed EPP in ref. (33). As it is known from the literature, the crystallization behavior of a polymer is influenced by the temperature profile, cooling rate, atmosphere, and more (34). All these factors influence the autoclave process and, thus, the foam properties such as density, cell size distribution, and crystal structure.

2.2.2 Processing behavior

To some extent, the influence of individual process conditions on bead properties has been studied. However, several conditions that might have an impact have not been fully considered in scientific literature. This chapter summarizes the influence of key process parameters (i.e., saturation pressure, saturation temperature, saturation time) and other factors such as the material type or the stirring speed inside the chamber.

2.2.2.1 Influence of saturation pressure

One of the first scientific publications dealing with the stirring autoclave process was focused on the influence of saturation pressure on thermal properties and foam morphology (33). Here, a PP-homopolymer and two PP-random copolymers (with PE and PE, PB) were used in the process. Before foaming, the pellets were processed into µ-granules with an average diameter of 0.6 mm. Due to the composition of these polymers, they had different melting ranges and therefore different foaming behaviors. The saturation pressure was varied between 30 and 60 bar for all polymers used. The resulting beads were analyzed in terms of their thermal behavior (i.e., melting peaks). It was found that as the saturation pressure increased (time and temperature were kept constant), the enthalpy for the higher melting peak decreased. This behavior is related to the plasticization effect, which is more pronounced as the pressure increases. A higher pressure leads to a more pronounced plasticization, due to the increased solubility, and therefore, a higher crystal fraction is melted. Consequently, only a few crystals are remaining which reorganize themselves to crystals with higher perfection. Although this behavior was observed, no correlation between the crystallinity and the processing conditions became evident.

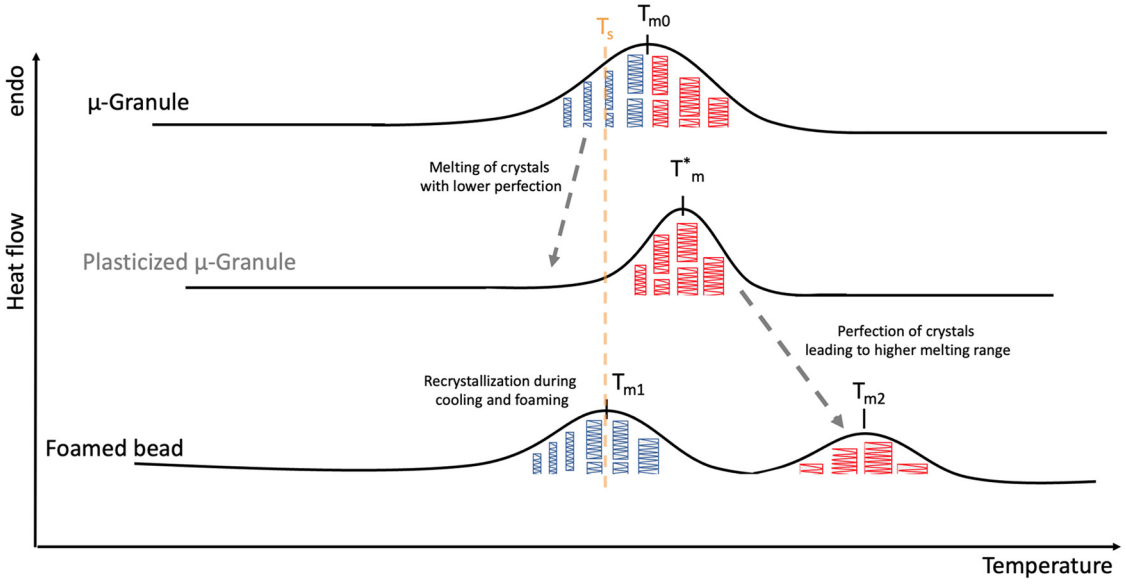

Figure 4: Proposed scheme of the transition from a single melting peak to a double melting peak structure during the autoclave processing. Lamella thickness are changing during the process. Copyright © 2023; University of Bayreuth, Department of Polymer Engineering.

In addition to EPP, polylactide (EPLA) was also prepared by the stirring autoclave method and the saturation pressure was varied by Nofar et al. (16,35). PLA 8051D from NatureWorks LLC was studied with CO_2 as blowing agent at different saturation pressures of 30, 60, and 172 bar. Increasing the saturation pressure results into lower glass transition temperatures (30,31) as well as lower melting temperatures leading to lower processing temperatures. This behavior can be explained by the increasing plasticizing effect of CO_2 with increasing saturation pressure because the melting peak shifts to lower temperatures with higher pressures. With increasing saturation pressure, lower densities were obtained, which can be attributed to a higher amount of dissolved gas in the polymer and a lower stiffness of the matrix, facilitating cell growth. Finally, the change in morphology at different saturation temperatures was demonstrated. In addition, it has been reported that increasing the saturation pressure leads to smaller cell sizes and higher densities (16). The expansion ratio as well as the foam morphology for selected samples is shown in Figure 5.

The effect of saturation pressure on the thermal properties of PP was studied in detail by Nofar et al. (36) using a high-pressure DSC (HPDSC). The saturation time was varied between 10 and 90 min at a pressure of 45 bar at 140°C for a PP–PE random copolymer. With an HPDSC, it is possible to simulate crystallization under conditions similar to those in autoclaves to better describe the underlying mechanisms. Therefore, the results were similar to the previously described autoclave experiments (33). It was also possible to find a correlation between the saturation temperature and the saturation pressure for the polymer type used. It was shown that a similar peak ratio, in terms of enthalpy, can be reached as follows:

$$T_s = -0.17P_s + 147.6 \quad (1)$$

where T_s is the saturation temperature and P_s is the saturation pressure.

In summary, an increase in saturation pressure increases plasticization and thus leads to a decrease in processing temperatures. This trend has been reported in the literature for PP as well as PLA.

2.2.2.2 Influence of saturation temperature

In addition to the saturation pressure, many publications (15–17,33,35–37) also varied the saturation temperature. Guo et al. (33) studied the influence of saturation temperature on the resulting foam morphology of different types of PP. As an example, they showed the effect of saturation temperature on cell density and foam morphology for a PP–PE random copolymer. The saturation pressure was kept constant at 50 bar and temperatures 144°C, 146°C, 148°C, and 150°C. Here, the cell density increased with increasing saturation temperature from 144°C to 148°C. The cell density increased from 1.4×10^9 to 9.8×10^9 cells·cm^{-3}, respectively.

In contrast, Tang et al. (20) showed for PP/PLA blends that increasing the saturation temperature resulted in a decrease in cell density. Here, the volume expansion ratio

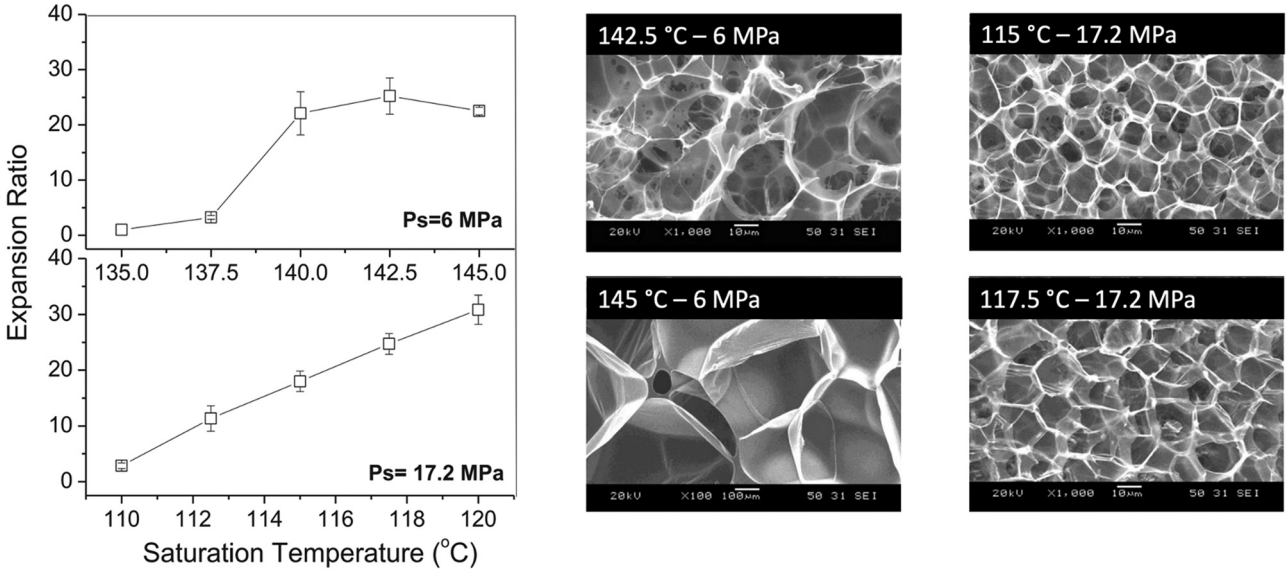

Figure 5: Variation of foaming pressure and temperature for EPLA bead foams and the corresponding foam morphology. Data are adapted with permission from ref. (16). Copyright © 2015; Elsevier Ltd. All rights reserved.

increased as well as the cell size increased. For EPC studied by Sánchez-Calderón et al. (17), the cell size (4–5 µm) and cell density (from 5×10^{10} to 1×10^{11} cells·cm^{-3}) remained almost constant with increasing saturation temperature, while the density decreased tremendously (from 592 to 126 kg·m^{-3}). In addition, it must be emphasized that PC crystallized during thermal treatment and foaming chains have time to crystallize. Figure 6 shows the bead foam morphologies made at various foaming temperatures.

For PLA, the effect of saturation temperature on density (volume expansion ratio) was investigated by Nofar et al. (15,16). In general, the density was lower with increasing temperature due to the lower stiffness of the matrix. The decrease in density with increasing saturation temperature was also shown for PP/PLA blends (20) and EPC (17). In addition, the thermal properties were evaluated. The second melting peak shifts to higher temperatures with increasing saturation temperature, while the enthalpy for the second melting peak and the total enthalpy of fusion decrease. These trends have been demonstrated for various saturation pressures from 30 to 172 bar (16). These effects have also been demonstrated for EPP (36) and EPC (17).

In general, it has been shown that the saturation temperature has a major influence on the foaming behavior. Increasing the saturation temperature can decrease the density, while the average cell size does not necessarily decrease. In addition to morphology, thermal properties are affected. To a certain extent, an increase in the saturation temperature leads to higher melting temperatures.

2.2.2.3 Influence of saturation time

Nofar et al. (36) studied the effect of saturation time on the formation of double melting peaks for a random PP copolymer. The saturation time was varied from 10 to 90 min at a fixed temperature of 140°C and a pressure of 45 bar. Low saturation times of 10 min resulted in insufficient peak separation due to insufficient time for crystal rearrangements. Longer saturation times of 20–90 min resulted in two clearly distinguishable melt peaks. In addition, the peak area ratio shifts to higher melt peak enthalpies. This phenomenon is due to the longer time for diffusion and rearrangement of the crystals. In addition, the enthalpy for the low melting peak decreases because a larger amount

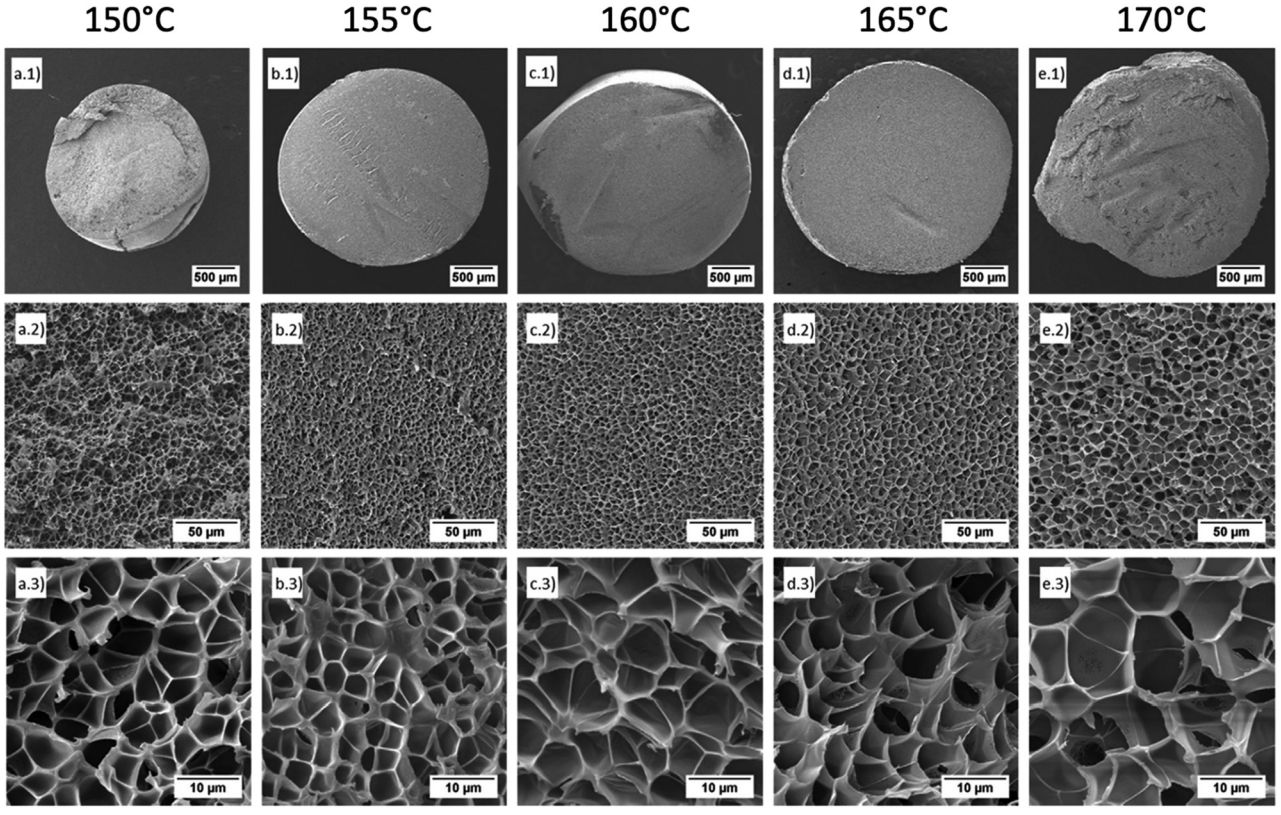

Figure 6: SEM images of different EPC bead foams produced at different temperatures between 155°C and 170°C at a pressure of 12 MPa for a saturation time of 30 min, the letter represents the processing parameter and the number the magnification. Data adapted with permission from ref. (17). Copyright © 2021; The Authors. Published by Elsevier Ltd.

is already crystallized as high melting peak. However, the overall crystallinity increases with saturation time.

In contrast to EPP, the effect of saturation time on bead properties has been studied for EPLA (15). A commercial grade of PLA from NatureWorks LLC (Ingeo 8051D) was modified with an epoxy-based chain extender. The saturation time was varied between 15 and 60 min at different temperatures and pressures. Increasing the saturation time resulted in crystals with a higher degree of perfection and thus a melting peak at higher temperatures. The greater number of perfect crystals promoted nucleation and led to an increase in overall crystallinity. However, a decrease in molecular weight was observed with increasing saturation time, which may be attributed to the sensitivity of PLA to hydrolysis. Interestingly, the expansion ratio increased with saturation time. This relationship is shown in Figure 7.

According to Nofar et al. (15), two effects influence the expansion. One effect is the lower molecular weight, which favors cell growth, and the other is the increased crystallinity, which increases rigidity and restricts expansion. In this case, the expansion ratio increased with saturation time, implying that the lower molecular weight had a greater effect on expansion than the more perfect crystals. However, the larger number of crystals supported cell nucleation, resulting in higher cell densities at higher saturation times. Additionally, the content of open cells at different saturation times was analyzed. Here, the higher saturation times resulted in higher open cell contents (OCC). The lower saturation time of 15 min resulted in an OCC of 15%, while the sample after 60 min had an OCC of approximately 90%. This was explained by the lower molecular weight (due to hydrolytic degradation) with increasing saturation time. Due to the lower molecular weight, the melt strength is reduced, and the strength of the cell walls is decreased, which allowed the cells to break more easily.

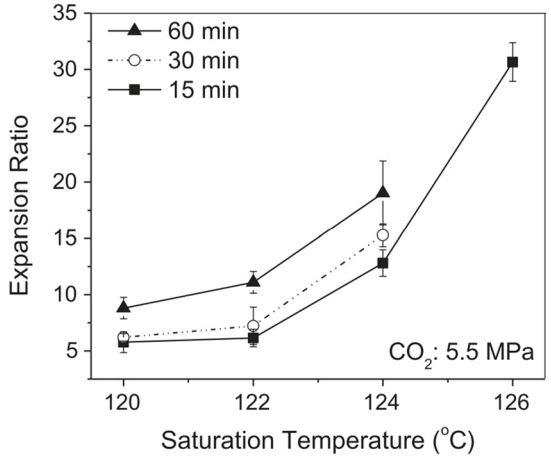

Figure 7: Expansion ratio of EPLA bead foams for different saturation times and temperatures. Data are adapted with permission from ref. (15).

Recently, EPC was also prepared in a stirring autoclave (17). Here, the saturation time was varied from 7.5 to 60 min at a temperature of 160°C and a pressure of 120 bar (CO_2). It was found that crystallinity increases with saturation time (up to 11% at 60 min saturation time, at 160°C and 120 bar), which explains the higher densities. The higher number of crystals leads to higher strength and thus to a limitation of expansion. However, the morphology (cell size and cell density) showed no significant influence on the saturation time.

The influence of saturation time on foaming behavior is well known. In the case of EPP, increasing the saturation time leads to more separated peaks. In the case of EPLA, increasing the saturation time leads to lower densities since PLA is susceptible to hydrolysis. Finally, for EPC, an increase in saturation time resulted in higher crystallinities that limited the expansion ratio but had no effect on the morphological properties. However, all these studies have shown that each material has its own characteristics, making it difficult to compare the effects between them. Additionally, the material properties are changing during the saturation process, which makes it even more complex to transfer knowledge from one to another material.

2.2.2.4 Other influencing parameters

In addition to temperature, time, and pressure during the saturation phase, other parameters are mentioned in the literature but are not described in detail. These include the influence of stirring speed during saturation, outlet geometry affecting the pressure drop rate, and the influence of material properties.

Only one publication (38) describes the influence of agitation speed on the distribution of the μ-granules during the process. The stirring speed was varied between 200 and 800 rpm. Up to a stirring speed of 400 rpm, the PP μ-granules are agglomerated. Thus, the buoyancy force of the particles is greater than the suction force of the stirrer. Higher stirring speeds resulted in good distribution in the autoclave. It was mentioned that the distribution and stirring speed depend on the stirrer geometry, but no details were given about the geometry used. The impact of stirring on heat distribution and the process itself was not studied in detail.

Another design parameter, the outlet geometry, influences the pressure drop rate and affects the foaming behavior (39). Guo et al. (38) varried the outlet by changing the nozzle length, which mainly affects the amount of beads discharged and the expansion ratio. Increasing the nozzle

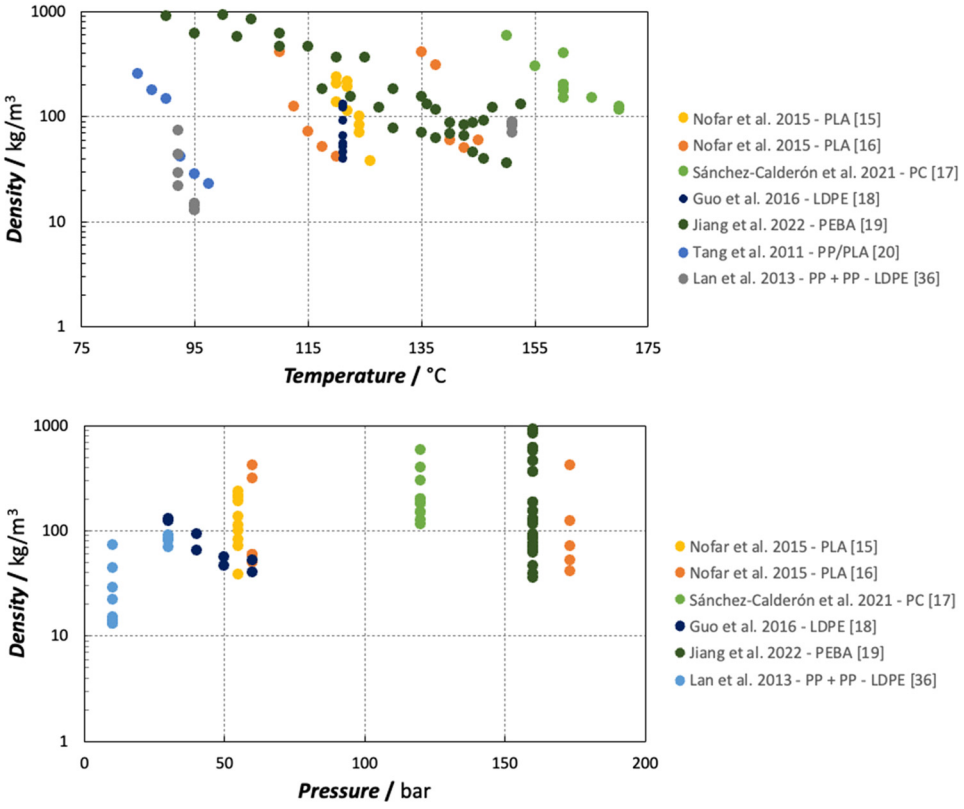

Figure 8: Comparison of density versus temperatures and pressures in scientific studies: (top) comparison of density vs pressure and (bottom) comparison of density vs temperature.

length resulted in incomplete discharge. In addition, the expansion ratio decreases linearly with nozzle length. In addition to these two effects, the die length also affects the crystalline structure. It was found that a longer die leads to an increase in the melting enthalpies. The melting peak at lower temperatures decreased slightly, while the melting peak at high temperatures increased. The increase in crystallinity was explained by higher shear-induced crystallization, which is more pronounced with longer dies.

In addition to the process parameters and the technical design, the material itself also has a great influence on the foaming performance, as known from several publications (16,20,33). Guo et al. (33) studied the foaming behavior of different PP-types. These types differ in composition (type of copolymer) and thus in the melting range, MFI (ranging from 2.2 up to 8.3 g·10 min^{-1}), and crystallinity. The processing window of these materials is depending on their thermal behavior. A higher melting range of the used polymer leads to higher processing temperature parameters in the autoclave process. But not only the material itself, the type of blowing agent affects the foaming performance. Lan et al. (37) foamed PP in the presence of CO_2 and pentane. They found that the use of pentane led to lower processing temperatures and high expansion ratios up to 50. In contrast to that, the use of CO_2 led to higher necessary foaming temperatures and lower expansion ratios up to 20.

The stirring speed, the outlet geometry, and different polymers have been investigated in autoclave processing (38). However, the stirring profile and outlet geometry were not studied, and no correlation was found when comparing different polymers. In addition, several parameters have not yet been studied, such as the heating profile during the saturation step or the cooling process after the particles are removed from the autoclave.

2.2.3 Overview of process parameters

Summarizing all the studies carried out on the production of bead foams using the stirring autoclave process, various polymers such as PP, PLA, or PC have been processed. However, depending on the polymer, the processing parameters are different. Therefore, an overview of selected properties is given in Figure 8. Here, each color stands for a publication. It should be mentioned that not all

publications provided the exact density data. These values were taken from diagrams or calculated from the volume expansion ratio and the density of the compact materials.

Comparing the density with the temperature profiles used, temperature and pressure were varied over a wide range in the studies. The studies show that the method can lead to very low densities below 10 $kg \cdot m^{-3}$. Regarding the temperature variations, density changes occur in a small temperature window, indicating the large influence of the processing temperature. Plotting density versus pressure, one can see that pressures from 10 to 172 bar have been studied in the literature. This shows that the bead foams can be produced over a wide range of saturation conditions. However, a single study investigating the pressure over a wide pressure range was not done so far.

In general, the stirring autoclave process has been studied by several research groups. However, there is still a lack of study on the correlation between several parameters and foam properties. To name one, the comparison of temperature and pressure with foam properties is crucial to enable highly efficient processes. Also, only static saturation parameters have been studied so far and more complex temperature and pressure regimes have not yet been considered in scientific literature.

2.3 Welding process of bead foams

After foamed beads are produced, they are welded into a final part according to the state of the art; the so-called SCM is mainly used. Steam acts as a heat source and enables rapid heat transfer and thus short cycle times (40,41). To give an overview about the welding process, first, the theoretical background is given, followed by the processing methods.

2.3.1 Theoretical background

To weld two polymers, a contact surface must be created. Subsequently, surface rearrangement and wetting occur (42). The welding itself is based on diffusion processes at the interfaces of the polymers to be welded. The diffusion of small molecules can be described by Fick's law. However, the welding of polymers is far more complex due to the chain structure of these polymers (43). Voyutskii produced one of the first descriptions of the adhesion behavior of polymer systems. Among other things, he showed the correlation between the contact time of the adhesive and the part to be bonded, the influence of the bonding temperature, and the influence of the molecular weight of the adhesive (44). From these results, Voyutskii concluded that diffusion plays an important role in the adhesive behavior of polymers (43–46).

Several models have been established based on assumptions about molecular structure. The model postulated by Rouse describes the diffusion of short-chain molecules and polymers below their critical entanglement molecular weight (42,47). Another established model, called the tube model (or reptation), was developed by de Gennes (48,49) and further modified by Doi and Edwards (50,51).

Figure 9 shows the reptation theory of de Gennes (52) at an interface for different time scales. The polymer chain is assumed to be in a tubular region. Due to Brownian motion, the polymer chain replicates forward and backward. After a characteristic time (t_{rep}), the polymer chain leaves the imaginary tube without forming restoring forces with respect to the initial state. When two polymers are welded, the polymers must interact across the interfaces. If two different polymers are used, the Flory interaction parameters affect the interdiffusion of the two polymers. For a high degree of interdiffusion, the polymers should ideally be miscible (43).

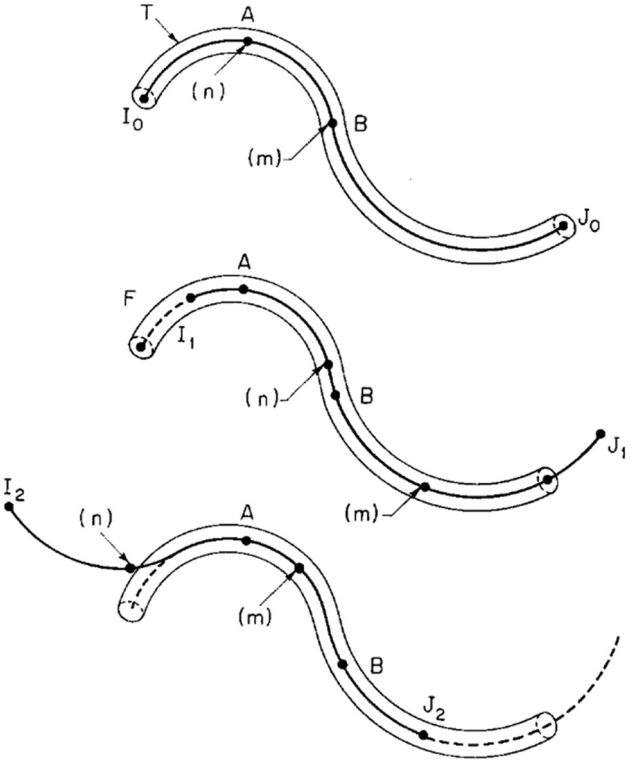

Figure 9: Chain movement of a polymeric macro molecule in fictitious tube. Data are adapted with permission from ref. (52). Copyright © 1998; American Chemical Society.

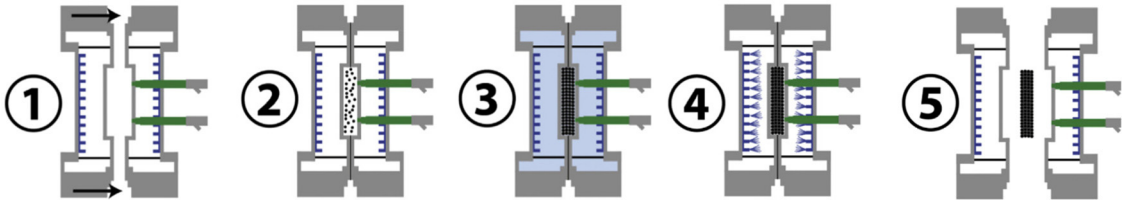

Figure 10: Steps of the SCM process. Data are adapted with permission from ref. (41). Copyright © 2014; Elsevier Ltd. All rights reserved.

The whole welding/interdiffusion process is time dependent and the corresponding models apply to different time scales. Between t_0 and t_e (characteristic Rouse relaxation time), the Rouse model is valid for small molecules. For diffusion times between t_e and t_R (characteristic Rouse relaxation time for the whole chain), the behavior follows the Rouse model. The region between t_R and t_{rep} follows the Doi–Edwards relaxation theory, and for diffusion times larger than t_{rep}, the process follows Fick's law (42,43). A more detailed description and corresponding equations can be found in other publications (42,43,47,49). It should be noted here that these relations apply to the description of amorphous matter systems.

2.3.2 Steam-based bead foam processing

In general, the process can be divided into five steps as shown in Figure 10: (i) closing the cavity, (ii) injecting the foamed beads, (iii) welding the foamed beads to a molded part with steam, (iv) cooling/stabilizing, and (v) ejecting the molded part (41). After closing the cavity, the foamed beads are injected into the mold with compressed air. The cavity is then preheated with steam flowing around. This is followed by a so-called cross-steam phase, in which steam flows through the filled cavity and provides the thermal energy required for surficial softening that enables (inter) diffusion of polymer chains across neighboring bead borders resulting in a physical bond (i.e., entanglement). This cross-steam phase is carried out horizontally in two directions to ensure uniform heating. Finally, an autoclave steam is used to improve surface quality. The steaming process is followed by a cooling step in which cold water is sprayed through nozzles to stabilize the molded part in the cavity. Depending on the size of the molded part, cycle times of 30 up to 90 s are common. The typical steam pressures used to produce EPP parts are between 2 and 4 bar, which corresponds to a steam temperature of approx. 130°C up to 150°C.

Three different methods can be used to fill the cavity. These are shown in Figure 11. Pressureless filling is the simplest method. Here, the bead foams are filled into the cavity by applying low pressures which are usually below 0.5 bar. Another method is pressure filling of the cavity with bead foams. The beads are transported into the cavity and pressurized (up to 4 bar) so that they are compressed in the mold, creating a large contact area between the beads. This method is often used for compressible materials like EPP with a density below 100 $kg \cdot m^{-3}$. The third method, which is also used for EPP, is the so-called crack-filling process. Here, the bead foams are filled into the cavity without counter pressure inside the mold. Immediately before SCM begins, the mold moves further and compresses the beads to achieve a high contact area. This

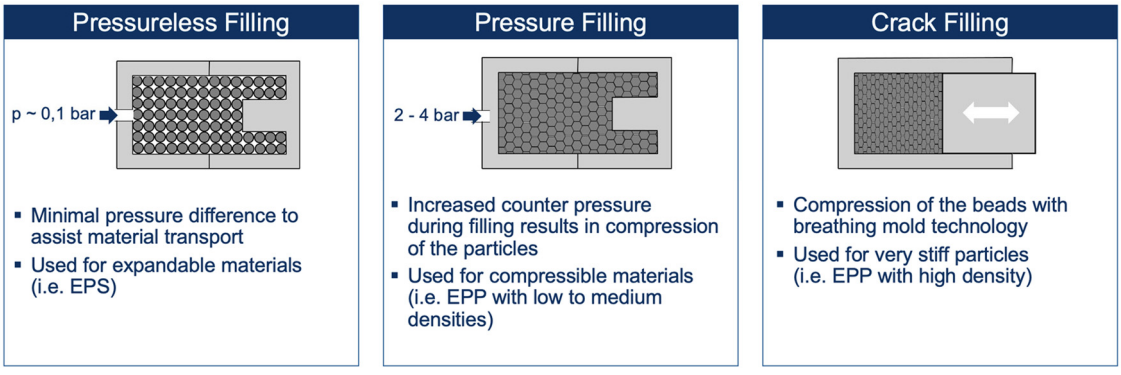

Figure 11: Overview of different filling methods for conducting the conventional SCM process (88). Copyright © 2023; Neue Materialien Bayreuth GmbH.

process is used for rigid materials, such as high-density EPP, which cannot be compressed by higher air pressure.

In the case of EPS, a blowing agent is still present in the bead, which evaporates due to heating during the fusion process and leads to post-foaming of the bead foam resulting in good contact between the loose beads (53). In the case of EPP, there is no more blowing agent in the bead, so it does not expand during the welding process. Therefore, the expanded beads are compressed before or during the welding process so that the gusset volume is reduced (i.e., the undesired voids between the beads) (53–56). Several studies have been conducted specifically on the processing of EPS. It was shown that the steam temperature and steaming time significantly affect the mechanical properties of the component (53). During the steaming process, the surface of the beads softens and allows interdiffusion of polymer chains between the two beads (16). Stupak et al. (57) show the relationship between fracture toughness and fusion parameters. Fracture toughness increased with steaming time proportional to $t^{1,25}$ and steaming pressure proportional to $p^{6,7}$. The deviations from the theoretical ratios are due to the non-ideal prevailing wetting and interdiffusion (41,57). If the steaming time is too long, the beads collapse and the surface and mechanical properties are negatively affected (57).

Thus, in EPS welding, sufficient chain mobility must be achieved by softening the polymer matrix. In the case of EPP, the phenomena are much more complex due to its semi-crystalline nature. To produce a good fusion in EPP, two melting peaks are usually created during the saturation step in the stirring autoclave. A schematic representation of the thermal properties and the welding profile is shown in Figure 12.

Based on Figure 12, the fusion temperature for semi-crystalline polymers lies between the two melting peaks. Here, the higher melting peak (T_{m2}) provides stability during fusion, while the lower melting peak (T_{m1}) provides the necessary chain mobility. During the fusion, crystals belonging to the lower melting peak are partially molten while the crystals of the high melting peak remain (16,54,55).

A study of the fusion and the evolution of the crystalline structures was carried out using AFM for EPP (58). Here, the weld line of a fused EPP part was investigated. It was shown that the weld line between the beads is homogeneous, and no interface is seen in the AFM anymore. The corresponding AFM and optical images are shown in Figure 13. These results indicate that under suitable conditions, interdiffusion and recrystallization occur at the interface during welding (58). These results are in good agreement with results from Zhai et al. (55), who mimicked the bead foam processing with a DSC.

Nofar transferred the concept of two distinct melting peaks to the processing and fusion of PLA-based bead foams (15,16). Here, EPLA was prepared using an autoclave process. Two melting peaks were created in PLA, allowing the beads to be fused together.

3 Mechanical properties of welded bead foam

In general, the resistance to deformation and failure of foams depend on the properties of the material the foam is made of, the relative density, and the cell structure (59).

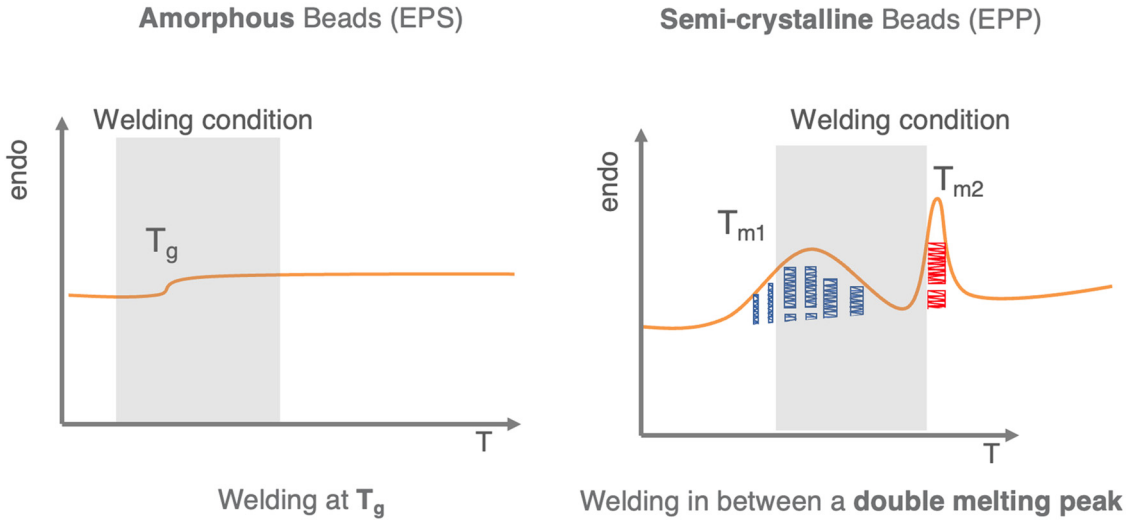

Figure 12: Fusion conditions for amorphous and semi-crystalline bead foams.

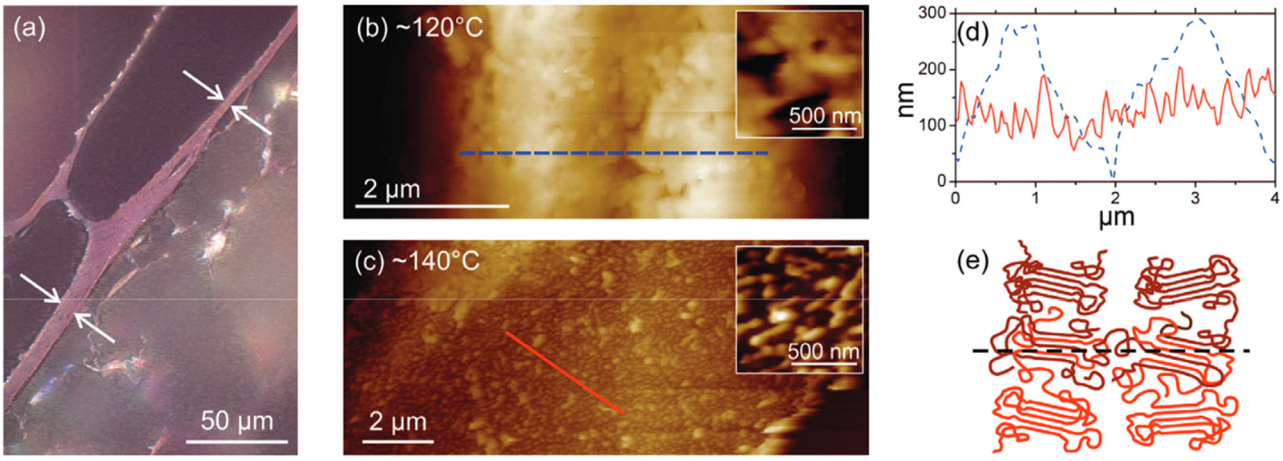

Figure 13: (a) Optical microscope image of the interface of two foamed and fused beads (marked by arrows). (b and c) AFM images showing the interface of two EPP foamed beads welded at 120°C and 140°C, respectively. (d) The corresponding height profiles after plasma etching to remove the amorphous regions across the bead interfaces. (e) Schematic of the presumed structure at the interface (including re- or co-crystallization in the interface). Data adapted with permission from ref. (58). Copyright © 2017; AIP Publishing.

The mechanical behavior of bead foams is far more complex than extrusion foams. To date, the number of publications dealing with the mechanical behavior of bead foams obtained from the stirring autoclave process is rather limited. However, the multi-step production process has a huge influence on the mechanical properties of these materials.

3.1 Cellular structure

Each process step has an impact on the final component and on its cell structure, which can be generally divided into a micro-, meso-, and macrostructure. Microstructure refers to the cellular structure within the beads, including the shape of the cells, the thickness of the cell walls, and the struts. Mesostructure includes the bead walls, and the size as well as the shape of the beads. Finally, the macrostructure describes the overall arrangement of the beads in the final product (60). Di Landro et al. showed that the size of the beads affects the mechanical properties. Analyzing the material with SEM, they found that the crushing of the EPS cells was localized at the boundaries between the beads. Based on these observations, it was concluded that the size of the pre-expanded beads may affect the deformation and energy absorption capacity of EPS. For a similar overall EPS density, smaller beads may result in a higher buckling load, and thus greater deformation and energy absorption capacity, than larger beads (61). Mills and Gilchrist studied various EPP bead foams with different bead sizes and densities. Using computational fluid dynamics,

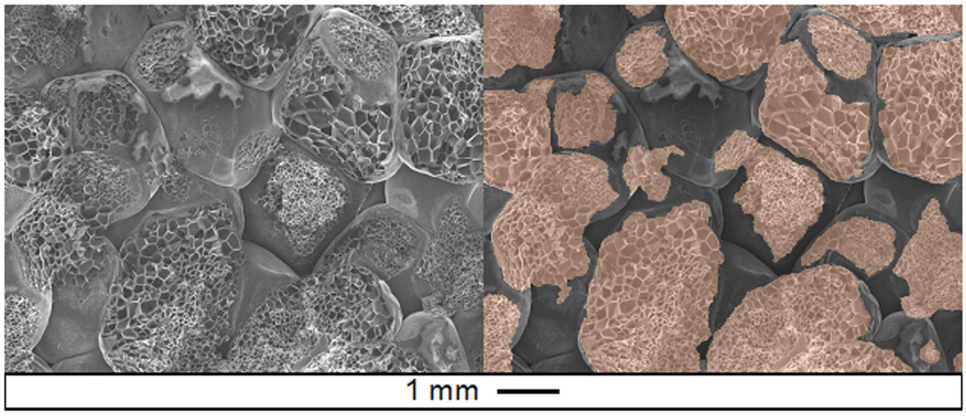

Figure 14: SEM images of the fracture surface after tensile tests on EPP (191 kg·m^{-3}). The right figure shows the trans-bead fracture surfaces in orange (see also ref. (66)).

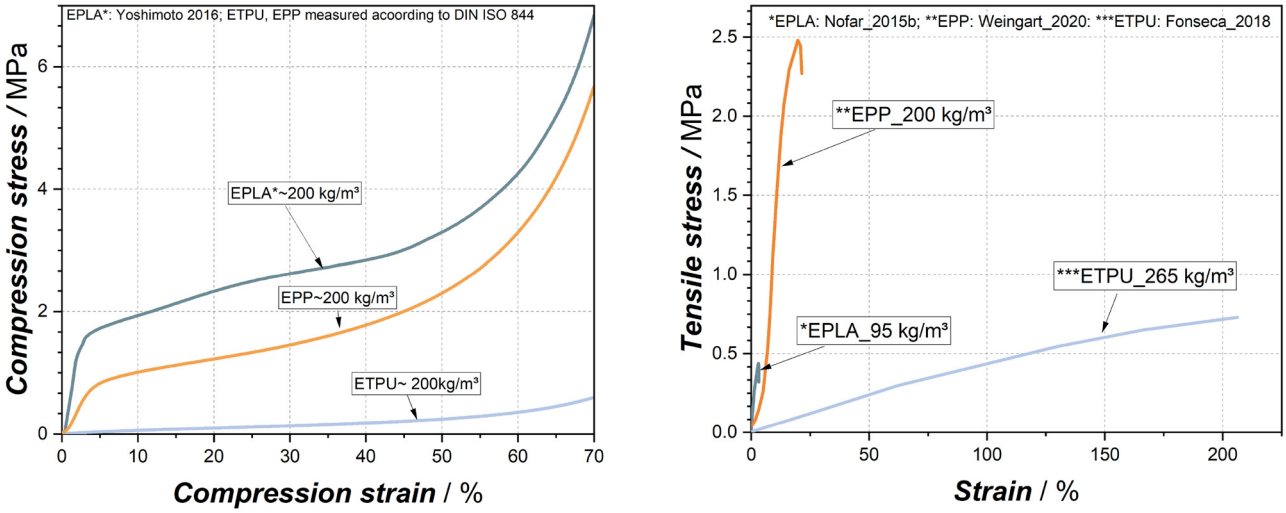

Figure 15: Comparison of the stress–strain curves in compression (left) and tensile (right) according to ref. (15,68,69).

they found that the air permeability of the foam increases with the square of the bead size and the 2.6th power of the measured porosity (62). In addition to macropores, mechanical properties are dominated by the welding quality and the density gradient due to the process (63–65).

Often three-point-bending tests or tensile tests are performed to analyze the fusion quality. Then, the fracture surface is analyzed by comparing the ratio between inter-bead and intra-bead (also called trans-bead) failures, as shown in Figure 14. The higher the percentage of internal bead failures, the better the fusion quality.

3.2 Influence of base material

In addition to the cell structure, the material from which the foam is made, the base material, has a great influence on the behavior of the foam. Figure 15 shows the compression and tensile stress–strain curves of EPP, EPLA, and ETPU produced in a stirring autoclave. The tensile and compressive properties of these foams vary widely. EPLA and EPP exhibit compression behavior typical of a plastic-elastic foam, while ETPU represents the category of elastic foams (67). By comparing the tensile stress–strain curves, the difference between the materials becomes even more apparent. As an example, the graph shows that EPLA has the highest stiffness, EPP has the highest tensile strength, and ETPU has the highest elongation at break (15,68,69). It should be noted that tensile stress–strain curves at comparable densities were not available for all three materials. In addition, EPLA is a non-commercial grade, suggesting the possibility of future improvements in its fusion quality. Because of the different mechanical behavior of the bead foams made of different base materials, there is a wide range of applications. EPP, for example, is widely used as a high-end packaging material, while ETPU is used as a cushioning material in sports shoes (41).

3.2.1 Influence of density

As mentioned above, the density affects the mechanical properties of foams in general. There is some work that addresses the density influence on the mechanical properties of EPP (60,64,70–74). The influence of the density on the compression behavior of EPP is exemplarily shown in Figure 16. It is evident that the mechanical properties like Young's modulus or plateau stress are depending on density.

Andena et al. (72) studied eight different densities in a range of 20–120 $kg{\cdot}m^{-3}$ to compare the results with the Ashby–Gibson model. They conclude that the model (67) adequately but not perfectly describes the dependence of the compressive modulus and plateau stress. It is assumed that there is a small process-induced anisotropy that affects the properties (72). Bouix et al. (64) studied the effects of strain rates from 10^{-2} to 10^{3} s^{-1} on the compression properties of six EPP foams with different densities from 35 to 150 $kg{\cdot}m^{-3}$. They found that higher densities led to an increase in collapse stress for the same strain rate, and higher strain rates resulted in higher collapse stress regardless of density. They hypothesized that the reason for this increase is caused by high strain rates. These high strain rates entrap the cell gas which counteracts the compression. Underwater imaging at different strain levels showed that less cell gas escapes at higher strain rates (64).

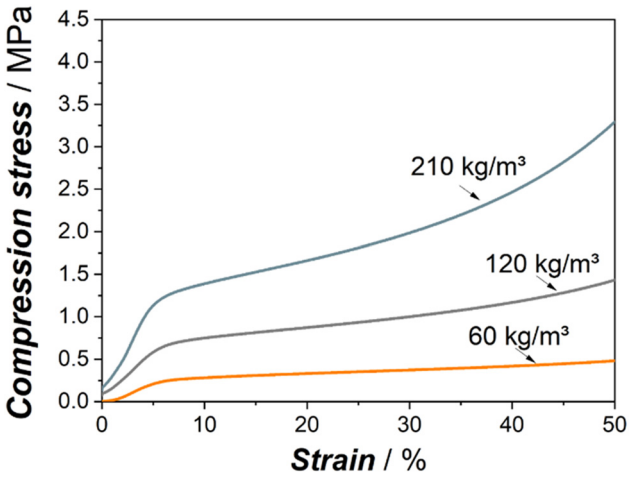

Figure 16: EPP with different densities according to ref. (70).

EPP foams are widely used in bumper cores and high-value packaging due to their high energy absorption potential (41). The energy absorption at different strain rates was investigated by Ruminek et al. (74) using experimental material tests of EPP with densities between 20 and 220 kg·m^{-3} and numerical simulations with ABAQUS. They concluded that both higher strain rates and higher densities lead to higher energy absorption capacity (74).

Ge et al. studied the density-dependent compressive and tensile behavior of ETPU with three different densities (i.e., 240, 290, and 350 kg·m^{-3}, respectively). As the density increases, the tensile and compressive properties of the foams increase. To investigate the recovery behavior, the specimens were compressed 200 times by 60%, followed by compression tests after 12, 72, and 144 h. The observed exceptional recovery behavior is shown in Figure 17 (75).

3.3 Influence of temperature

Bead foams are exposed to different ambient conditions during their service life. An interesting study from Morton et al. (76) describes the compression behavior of EPP over a temperature range from −30°C up to 60°C. It was found that the collapse stress, which describes the transition point between linear-elastic and plateau regime, increases by 110% at −30°C and decreases by 50% at 60°C compared to 23°C. The compression and tensile curves at different temperatures are shown in Figure 18.

Adequate testing of thermoplastic bead foams at different temperatures is challenging due to the large differences in foam structure, density, and low thermal conductivity. Himmelsbach et al. (70) developed an engineering approach to minimize these effects. Herein, it was proposed to determine the so-called heat stability temperature T_{HS} of (extrusion and bead) foams with a two-stage test. In the first stage, the basic compression behavior at room temperature (according to DIN EN ISO 844) is evaluated to define an individual test load, which is applied during the second stage – a creep test with step-wise increased thermal load. Different from other test methods, using this approach the influences of the foam density and the thermal inertia caused by the cellular structure are significantly reduced. In Figure 19 the results for different foams are summarized; the T_{HS} for polystyrene foams is approx. 98°C. For EPP from the stirring autoclave (with different densities), a narrow range of 99–107°C was measured while a bead foam made from polybutylene therephthalate (E-PBT) exhibits a T_{HS} of 186°C.

Besides the quasi-static properties dynamic properties are of great importance. However, the literature on this

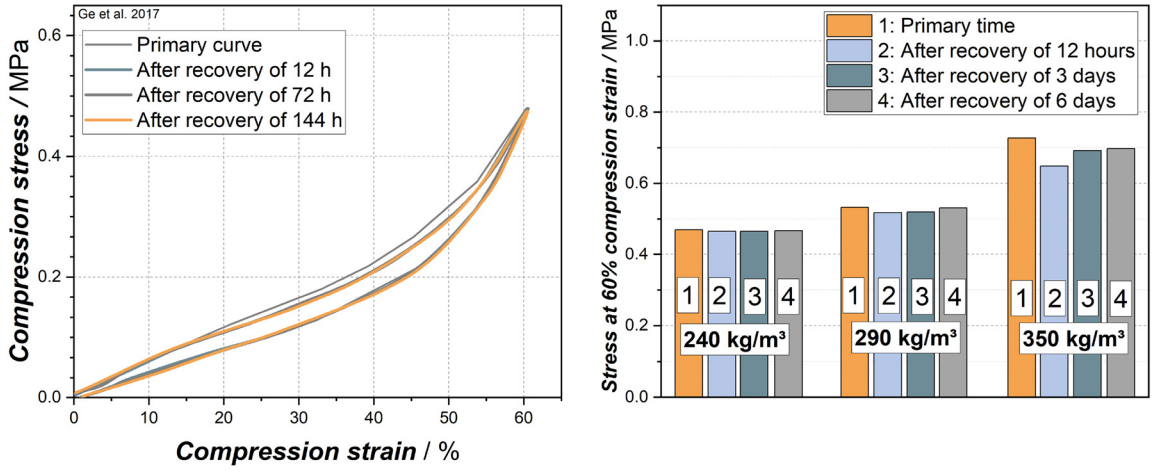

Figure 17: Compression curve (left) and recovery behavior (right) of different dense ETPU bead foams according to ref. (75).

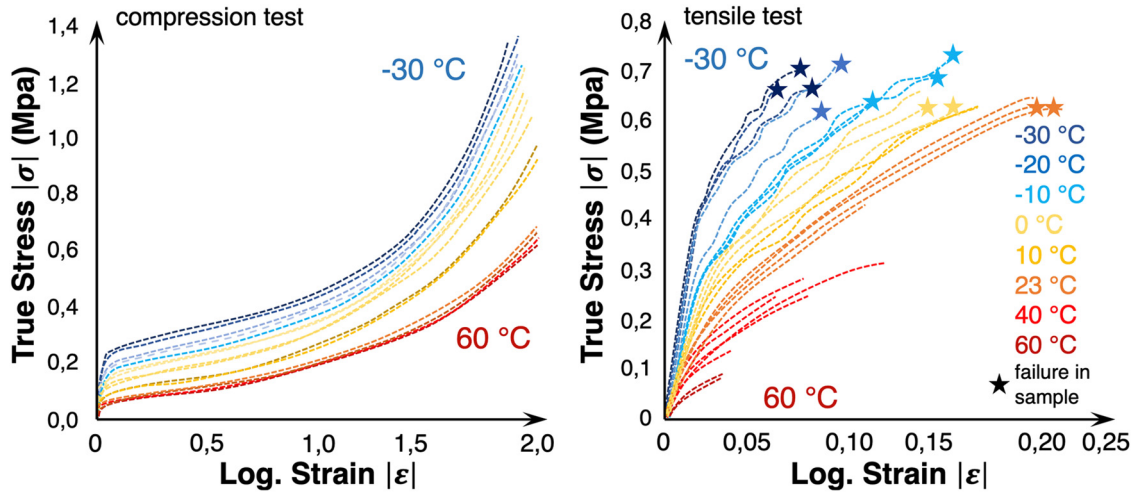

Figure 18: Compression tests (left) and tensile tests (right) of EPP (28 kg·m^{-3}) at different temperatures ranging from −30°C to 60°C according to ref. (76).

field is quite limited. The fatigue behavior of foams has hardly been studied so far. Keller and Altstädt (77) investigated the influence of compressive midstress on the fatigue behavior of EPS. It was shown that the mechanical behavior changed from a linear behavior to "a kind of exponential" behavior after a certain dynamic load.

4 Future trends

4.1 Digitalization

Digitization is still a comparatively young subfield of materials science but is currently gaining increasing attention. Kimmig et al. (78) summarized the potential of digitization in a recent review. Digital methods include machine learning (ML), deep learning, simulation, and modeling. Recently, a review of the application of ML to polymer design, identification, modeling, analysis, and characterization was published (79). However, little research has been done on the application of ML to polymer processing for optimization of the process parameter or the material properties.

Overall, there is little activity in the field of digital methods related to bead foams. The ILK Dresden is working with modeling and simulation to describe the complex mechanical behavior of bead foams, which is determined not only by the foam structure but also by the higher-level structure of the bead interfaces. So-called Voronoi mosaics can be used to take into account aspects such as

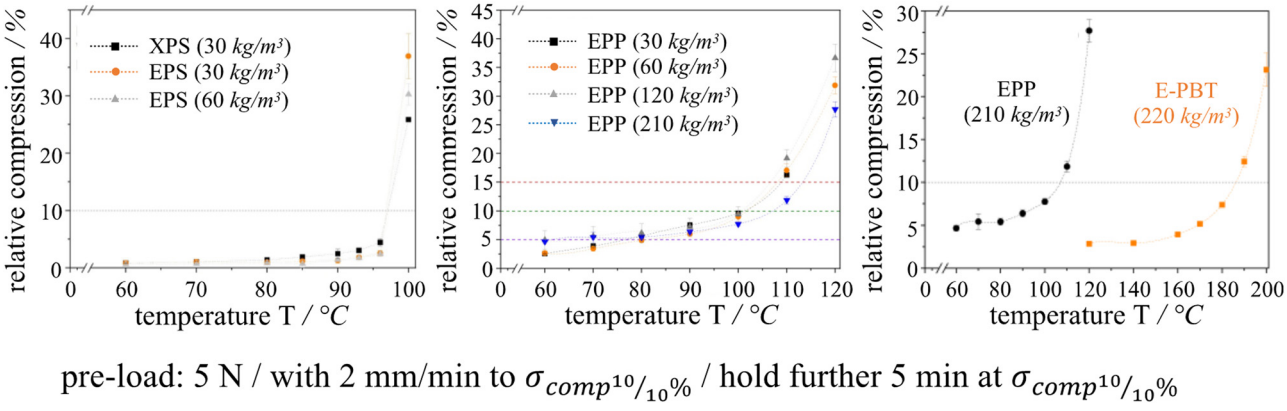

Figure 19: Heat stability temperatures T_{HS} obtained from a novel approach using steady creep tests with temperature steps for: (left) polystyrene foams (extrusion and bead foams with different densities), (mid) EPP with different densities, and (right) EPP and E-PBT at a density above 200 kg·m^{-3} according to ref. (70).

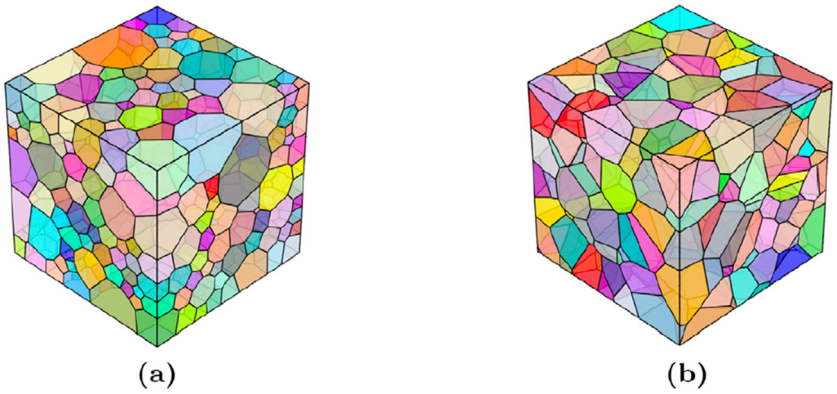

Figure 20: Tessellation of a statistical volume element visualizing the Grain-growth and Voronoi models. Data are adapted with permission from ref. (60). Copyright © 2019; Elsevier Ltd. All rights reserved. (a) Grain growth model, and (b) Voronoi models.

inhomogeneities of the cell structure and density when describing the compression behavior (80–82). Besides the Voronoi model, the Grain-growth model exists; both showed good agreement with experimental data (60). Figure 20 represents a tessellation of a cube according to the Grain-growth and Voronoi-models.

The work of Nakai et al. (56) focuses on the welding of the molded part, here with emphasis on the steaming step and its effects, including heat transport effects and post-expansion. Albuquerque et al. (83) showed the potential of using different ML techniques in predicting foam densities as a function of polymer type and processing parameters. However, to date, it is still a challenge to collect enough data for ML foam processing applications.

4.2 Sustainability

Another trend that is emerging in both industry and academia is the use of bio-based materials and the reduction of the carbon footprint. Therefore, in recent years, there has been more research in the field of PLA. Among others, there are some works dealing with the foaming behavior of PLA in a stirring autoclave process like EPP (15,84). In addition, PHBV bead foams have been produced (85). However, none of these bead foams has yet been established in the market as a real alternative to EPP or EPS. For this reason, research in the field of bio-based polymers is still wide.

Another area of sustainability is the recycling of bead foams. Some publicly funded projects are looking at the product life cycle of EPP components and recyclability. In addition, JSP announced the commercialization of an EPP containing 15% recycled waste in 2020 (86) and with almost 100% recycled content in 2022 (87). Since these recycling processes are costly and affect the properties of the base resin, the whole process is affected. Therefore, research is needed to understand the degradation processes and how they affect the processing behavior and foam properties.

5 Conclusions

The use of bead foams has increased in recent decades. In particular, the stirring autoclave process for the production of foamed beads is still of great interest to the industry and by now is still the predominant process to obtain EPP. This review article gives an overview of the process in terms of principles of operation, the influence of processing parameters, fusion of molded parts, and mechanical properties. As the first review paper on this topic, the article gives an overview of the complete process chain.

The basic principle of the process is explained, followed by the conventional methods of bead foam bonding. In addition, the available studies were evaluated to gain knowledge about the different parameters. The saturation conditions, namely the time, temperature, and pressure, are crucial to tune the thermal behavior of the foamed beads. The saturation time influences the peak ratio leading to higher enthalpies of the high melting peak with increasing saturating time. The pressure itself is mainly changing the processing range due to the influence on the plasticization of the polymer. The processing temperature is affecting the crystal structure as well as the morphology. It was shown that a change in a few Kelvins leads to a tremendous change in cell sizes and peak ratios. In a few scientific works it could be shown, how the double melting peak that is created during the saturation phase can be influenced in terms of its extent and ratio. It is noteworthy that the literature only describes static saturation conditions (i.e., constant temperatures and pressures during the saturation period). Besides the

experiments in the autoclave, experiments with HPDSC were described in literature to gain a better understanding of the ongoing processes during the saturation and the underlying mechanisms, especially in terms of the crystallization. Yet, the formation of the double melting peak is still seen as a major precondition for a good fusion of the beads during the welding, determining a good mechanical performance (e.g., compression behavior). Both EPP and ETPU can be obtained from the stirring autoclave process and exhibit an advanced mechanical performance compared to EPS in terms of repeated loading and elasticity.

Although this process is of great interest to the industry, there are only few scientific papers, indicating a need for research. In particular, the areas of bio-based and high-temperature bead foams are of great interest due to regulations and new processing methods. Sustainability and digitalization will also play a more important role in the future, similar to other material fields.

Acknowledgements: We acknowledge all students who were involved in collecting and reviewing the literature. Also, we would like to thank Annika Pfaffenberger for the images of the microgranules. Furthermore, we thank the colleagues at the department for their input. The support of Bavarian Polymer Institute is further acknowledged.

Funding information: This study was funded by the Deutsche Forschungsgemeinschaft (DFG, German Research Foundation) – 491183248 and projects with the grant numbers RU2586/5-1, AL474/49-1, and AL474/45-1 and funded by the Open Access Publishing Fund of the University of Bayreuth.

Author contributions: Christian Brütting: writing – original draft, writing – review and editing; Tobias Standau: writing – original draft, writing – review and editing; Johannes Meuchelböck: writing – original draft; Peter Schreier: writing – original draft; Holger Ruckdäschel: writing – review and editing, project administration.

Conflict of interest: Authors state no conflict of interest.

References

(1) Stastny F, Gaeth R. Verfahren Zur Herstellung Poroeser Massen Aus Polymerisaten. German Pat., DE 845264C, 1950.
(2) Hiroyuki A, Kuninori H, Hideki K. Process for Producing Foamed and Moulded Article of Polypropylene Resin. US Pat., 4440703A, 1982.
(3) Rubens LC, Willard E, Anderson PE. Molding Expandable Thermoplastic Resins. US Pat., 4108934, 1978.
(4) Kuhnigk J, Standau T, Dörr D, Brütting C, Altstädt V, Ruckdäschel H. Progress in the development of bead foams – A review. J Cell Plast. 2022;58:707–35. doi: 10.1177/0021955X221087603.
(5) Expandable Polystyrene Market Report, 2032. https://ceresana.com/en/produkt/expandable-polystyrene-market-report (accessed on 31 March 2023).
(6) Expanded Polystyrene (EPS) Market Size & Trends to 2033. https://www.factmr.com/report/4080/expanded-polystyrene-market (accessed on 31 March 2023).
(7) Tammaro D, Ballesteros A, Walker C, Reichelt N, Trommsdorff U. Expanded beads of high melt strength polypropylene moldable at low steam pressure by foam extrusion. Polymers (Basel). 2022;14:205. doi: 10.3390/polym14010205.
(8) Tölle F. The future is now. Particle Foam 2018. Dusseldorf: VDI Verlag; 2018. p. 21–30.
(9) Expanded Polypropylene Foam Market Size Report, 2030 Available online: https://www.grandviewresearch.com/industry-analysis/expanded-polypropylene-epp-foam-market (accessed on 31 March 2023).
(10) Market Research Report, Expanded Polystyrene Market Size, Share & Trends Analysis Report by Product (White, Grey), by Application (Construction, Automotive, Packaging), by Region (APAC, Europe), and Segment Forecasts, 2021 8; 2021;
(11) Tokoro K, Tsurugai H, Masaharu O. Foamed Particles of Polypropylene Homopolymer and Molded Article of the Foamed Particles. US Patent US 5,747,549 A; 1996.
(12) Mair G, Nöthe A, Lambert J, Keppeler U, Schnorpfeil C. Verfahren Zur Herstellung von Polyolefin-Schaumstoffpartikeln. European Patent EP 2,336,225 A1; 2010.
(13) Kuwabara H. Process for the Production of Expanded Particles of a Polypropylene Resin. US Patent US 4,676,939; 1985.
(14) Braun F, Prissok US20100222442A1 F. Foams Based on Thermoplastic Polyurethanes. US Patent US 2010/0222442 A1; 2010.
(15) Nofar M, Ameli A, Park CB. A novel technology to manufacture biodegradable polylactide bead foam products. Mater Des. 2015;83:413–21. doi: 10.1016/j.matdes.2015.06.052.
(16) Nofar M, Ameli A, Park CB. Development of polylactide bead foams with double crystal melting peaks. Polymer (Guildf). 2015;69:83–94. doi: 10.1016/j.polymer.2015.05.048.
(17) Sánchez-Calderón I, Bernardo V, Martín-de-León J, Rodríguez-Pérez MÁ. Novel approach based on autoclave bead foaming to produce expanded polycarbonate (EPC) bead foams with microcellular structure and controlled crystallinity. Mater Des. 2021;212:110200. doi: 10.1016/j.matdes.2021.110200.
(18) Guo P, Xu Y, Lu M, Zhang S. Expanded linear low-density polyethylene beads: Fabrication, melt strength, and foam morphology. Ind Eng Chem Res. 2016;55:8104–13. doi: 10.1021/acs.iecr.6b01545.
(19) Jiang J, Liu F, Chen B, Li Y, Yang X, Tian F, et al. Microstructure development of PEBA and its impact on autoclave foaming behavior and inter-bead bonding of EPEBA beads. Polymer (Guildf). 2022;256:125244. doi: 10.1016/j.polymer.2022.125244.
(20) Tang L, Zhai W, Zheng W. Autoclave preparation of expanded polypropylene/poly(Lactic Acid) blend bead foams with a batch foaming process. J Cell Plast. 2011;47:429–46. doi: 10.1177/0021955X11406004.
(21) Ellouze A, Jesson D, Ben Cheikh R. The effect of thermal treatment on the properties of expanded polystyrene. Polym Eng Sci. 2020;60:2710–23. doi: 10.1002/PEN.25502.
(22) BASF Neopor® – a Raw Material for Diverse Solutions; https://neopor.de/portal/load/fid1225927/Neopor_Thermal_insulation.pdf available.

(23) BASF Neopolen® (EPP) Available online: https://plastics-rubber.basf.com/global/de/performance_polymers/products/neopolen.html (accessed on 21 March 2023).
(24) BASF The First Expanded TPU – As Elastic as Rubber but Lighter file:///Users/bt305444/Downloads/InfinergyEN_updated- 1.pdf.
(25) Sasaki H, Sakaguchi M, Akiyama M, Tokoro H. Expanded polypropylene resin beads and a molded Article 1998. US Patent US 6,313,184 B1.
(26) Yoshida T, Fukuzawa J, Imai T, Mori K, Tsuneishi H. Process for producing expanded polyolefin resin particles and expanded polyolefin resin particles 2008. European Patent EP 2,754,687 B1.
(27) Frank Braun. Guiscard Glick; Klaus Hahn; Isidoor De Grave; Hermann Tatzel expanded polypropylene particles. US Patent US 6,677,040 B1; 2004.
(28) Mair G, Nöthe A, Lambert J, Keppeler U, Schnorpfeil C. Process for Producing Polyolefin Foam Particles. US Patent US 6,677,040 B1; 2010.
(29) Nofar M, Tabatabaei A, Ameli A, Park CB. Comparison of melting and crystallization behaviors of polylactide under high-pressure CO_2, N_2, and He. Polymer (Guildf). 2013;54:6471–8. doi: 10.1016/j.polymer.2013.09.044.
(30) Brütting C, Dreier J, Bonten C, Altstädt V, Ruckdäschel H. Glass transition of PLA-CO 2 mixtures after solid-state saturation. J Cell Plast. 2022;58:917–31. doi: 10.1177/0021955X221144543.
(31) Takada M, Hasegawa S, Ohshima M. Crystallization kinetics of poly (L-lactide) in contact with pressurized CO2. Polym Eng Sci. 2004;44:186–96. doi: 10.1002/pen.20017.
(32) Hingmann R, Rieger J, Kersting M. Rheological properties of a partially molten polypropylene random copolymer during Annealing. Macromolecules. 1995;28:3801–6. doi: 10.1021/ma00115a008.
(33) Guo P, Liu Y, Xu Y, Lu M, Zhang S, Liu T. Effects of saturation temperature/pressure on melting behavior and cell structure of expanded polypropylene bead. J Cell Plast. 2014;50:321–35. doi: 10.1177/0021955X14525798.
(34) Nofar M, Tabatabaei A, Ameli A, Park CB. Comparison of melting and crystallization behaviors of polylactide under high-pressure CO_2, N_2, and He. AIP Conf. Proc. 2014;1593:320–3. doi: 10.1063/1.4873791.
(35) Nofar M, Ameli A, Park CB. Expanded polylactide bead foaming – A New Technology. AIP Conf. Proc; 2015 1664. doi: 10.1063/1.4918400.
(36) Nofar M, Guo Y, Park CB. Double crystal melting peak generation for expanded polypropylene bead foam manufacturing. Ind Eng Chem Res. 2013;52:2297–303. doi: 10.1021/ie302625e.
(37) Lan X, Zhai W, Zheng W. Critical effects of polyethylene addition on the autoclave foaming behavior of polypropylene and the melting behavior of polypropylene foams blown with N-Pentane and CO2. Ind Eng Chem Res. 2013;52:5655–65. doi: 10.1021/ie302899m.
(38) Guo Y, Hossieny N, Chu RKMM, Park CB, Zhou N. Critical processing parameters for foamed bead manufacturing in a lab-scale autoclave system. Chem Eng J. 2013;214:180–8. doi: 10.1016/j.cej.2012.10.043.
(39) Standau T, Long H, Murillo Castellón S, Brütting C, Bonten C, Altstädt V. Evaluation of the zero shear viscosity, the D-content and processing conditions as foam relevant parameters for autoclave foaming of standard polylactide (PLA). Materials (Basel). 2020;13:1371. doi: 10.3390/ma13061371.
(40) Kuhnigk J, Krebs N, Standau T, Dippold M, Ruckdäschel H, Kuhnigk J, et al. Evaluation of the fusion quality of bead foams made from polybutylene terephthalate (E-PBT) depending on the processing temperature. Macromol Mater Eng. 2022;307:2200419. doi: 10.1002/MAME.202200419.
(41) Raps D, Hossieny N, Park CB, Altstädt V. Past and present developments in polymer bead foams and bead foaming technology. Polymer (Guildf). 2015;56:5–19. doi: 10.1016/j.polymer.2014.10.078.
(42) Wool RP, Yuan BLL, McGarel OJ. Welding of polymer interfaces. Polym Eng Sci. 1989;29:1340–67. doi: 10.1002/pen.760291906.
(43) Bousmina M, Qiu H, Grmela M, Klemberg-Sapieha JE. Diffusion at Polymer/Polymer Interfaces Probed by Rheological Tools. Macromolecules. 1998;31(23):8273–80. doi: 10.1021/ma980562r.
(44) Voyutskii SS, Vakula VL. The Role of Diffusion Phenomena in Polymer-to-polymer Adhesion. J Appl Polym Sci. 1963;7:475–91. doi: 10.1002/APP.1963.070070207.
(45) Voyutskii SS. Some comments on the series of papers “interfacial contact and bonding in autohesion. J Adhes. 1971;3:69–76. doi: 10.1080/00218467108075007.
(46) Kinloch AJ. Adhesion and adhesives. 1st ed. Dordrecht: Springer Netherlands; Vol. 1987.
(47) Rouse PE. A theory of the linear viscoelastic properties of dilute solutions of coiling polymers. J Chem Phys. 1953;21:1272–80. doi: 10.1063/1.1699180.
(48) De Gennes PG. Dynamics of entangled polymer solutions. I. The Rouse model. Macromolecules. 1976;9:587–93. doi: 10.1021/ma60052a011.
(49) de Gennes PG. Reptation of a polymer chain in the presence of fixed obstacles. J Chem Phys. 1971;55:572–9. doi: 10.1063/1.1675789.
(50) Doi M, Edwards SF. Dynamics of rod-like macromolecules in concentrated solution. Part 1. J Chem Soc Faraday Trans 2 Mol Chem Phys. 1978;74:560–70. doi: 10.1039/F29787400560.
(51) Doi M, Edwards SF. Dynamics of rod-like macromolecules in concentrated solution. Part 2. J Chem Soc Faraday Trans 2 Mol Chem Phys. 1978;74:918–32. doi: 10.1039/F29787400918.
(52) de Gennes PG. Reptation of a polymer chain in the presence of fixed obstacles. J Chem Phys. 1971;55:572–9. doi: 10.1063/1.1675789.
(53) Rossacci J, Shivkumar S. Bead fusion in polystyrene foams. J Mater Sci. 2003;38:201–6. doi: 10.1023/A:1021180608531.
(54) Zhai W, Kim Y-W, Jung DW, Park CB. Steam-Chest molding of expanded polypropylene foams. 2. mechanism of interbead bonding. Ind Eng Chem Res. 2011;50:5523–31. doi: 10.1021/ie101753w.
(55) Zhai W, Kim YW, Park CB. Steam-chest molding of expanded polypropylene foams. 1. dsc simulation of bead foam processing. Ind Eng Chem Res. 2010;49:9822–9. doi: 10.1021/ie101085s.
(56) Nakai S, Taki K, Tsujimura I, Ohshima M. Numerical Simulation of a polypropylene foam bead expansion process. Polym Eng Sci. 2008;48:107–15. doi: 10.1002/pen.20895.
(57) Stupak PR, Frye WO, Donovan JA. The effect of bead fusion on the energy absorption of polystyrene foam. part i: fracture toughness. J Cell Plast. 1991;27:484–505. doi: 10.1177/0021955X9102700503.
(58) Gensel J, Pawelski C, Altstädt V. Welding quality in polymer bead foams: an *in situ* SEM study. In: Proceedings of the AIP Conference Proceedings; American Institute of Physics Inc. Vol. 1914; December 14 2017. p. 060001.
(59) Ashby MF. The properties of foams and lattices. Philos Trans R Soc A Math Phys Eng Sci. 2006;364:15–30. doi: 10.1098/rsta.2005.1678.
(60) Gebhart TMJ, Jehnichen D, Koschichow R, Müller M, Göbel M, Geske V, et al. Multi-scale modelling approach to homogenise the mechanical properties of polymeric closed-cell bead foams. Int J Eng Sci. 2019;145:103168. doi: 10.1016/j.ijengsci.2019.103168.
(61) Di Landro L, Sala G, Olivieri D. Deformation mechanisms and energy absorption of polystyrene foams for protective helmets. Polym Test. 2002;21:217–28. doi: 10.1016/S0142-9418(01)00073-3.

(62) Mills N. Polymer foams handbook engineering and biomechanics applications and design. Boston: Guide Butterworth-Heinemann; 2007.
(63) Hossieny N, Ameli A, Park CB. Characterization of expanded polypropylene bead foams with modified steam-chest molding. Ind Eng Chem Res. 2013;52:8236–47. doi: 10.1021/ie400734j.
(64) Bouix R, Viot P, Lataillade J-L. Polypropylene foam behaviour under dynamic loadings: strain rate, density and microstructure effects. Int J Impact Eng. 2009;36:329–42. doi: 10.1016/j.ijimpeng.2007.11.007.
(65) Moosa AS, Mills N. Analysis of bend tests on polystyrene bead foams. Polym Test. 1998;17:357–78. doi: 10.1016/S0142-9418(97)00063-9.
(66) Standau T, Schreiers P, Hilgert K, Altstädt V. Properties of bead foams with increased heat stability made from the engineering polymer polybutylene terephthalate (E-PBT); 2020. p. 020039.
(67) Gibson LJ, Ashby MF. Cellular Solids: Structure and Properties, Second Edition. Cambridge: Cambridge University Press; 2014.
(68) Weingart N, Raps D, Kuhnigk J, Klein A, Altstädt V. Expanded polycarbonate (EPC) – A new generation of high-temperature engineering bead foams. Polymers (Basel). 2020;12:2314. doi: 10.3390/polym12102314.
(69) Fonseca I, Bräuer J, Graessel G, Hennenberger F, Birli R, Gutmann P. Advances in high performance thermoplastic foams results and discussion. In: Proceedings of the SPE Foams; 2018.
(70) Himmelsbach A, Standau T, Meuchelböck J, Altstädt V, Ruckdäschel H. Approach to quantify the resistance of polymeric foams against thermal load under compression. J Polym Eng. 2022;42:277–87. doi: 10.1515/polyeng-2021-0312.
(71) Beverte I. Deformation of polypropylene foam neopolen® P in compression. J Cell Plast. 2004;40:191–204. doi: 10.1177/0021955X04043718.
(72) Andena L, Caimmi F, Leonardi L, Nacucchi M, De Pascalis F. Compression of polystyrene and polypropylene foams for energy absorption applications: a combined mechanical and microstructural study. J Cell Plast. 2019;55:49–72. doi: 10.1177/0021955X18806794.
(73) Mills NJ, Gilchrist A. Properties of bonded-polypropylene-bead foams: data and modelling. J Mater Sci. 2007;42:3177–89. doi: 10.1007/s10853-006-1357-0.
(74) Rumianek P, Dobosz T, Nowak R, Dziewit P, Aromiński A. Static mechanical properties of expanded polypropylene crushable foam. Materials (Basel). 2021;14:249. doi: 10.3390/ma14020249.
(75) Ge C, Ren Q, Wang S, Zheng W, Zhai W, Park CB. Steam-chest molding of expanded thermoplastic polyurethane bead foams and their mechanical properties. Chem Eng Sci. 2017;174:337–46. doi: 10.1016/j.ces.2017.09.011.
(76) Morton DT, Reyes A, Clausen AH, Hopperstad OS. Mechanical response of low density expanded polypropylene foams in compression and tension at different loading rates and temperatures. Mater Today Commun. 2020;23:100917. doi: 10.1016/J.MTCOMM.2020.100917.
(77) Keller J-H, Altstädt V. Influence of Mid-stress on the dynamic fatigue of a light weight EPS bead foam. e-Polymers. 2019;19:349–54. doi: 10.1515/epoly-2019-0036.
(78) Kimmig J, Zechel S, Schubert US. Digital transformation in materials science: A Paradigm change in material's development. Adv Mater. 2021;2004940. doi: 10.1002/adma.202004940.
(79) Sha W, Li Y, Tang S, Tian J, Zhao Y, Guo Y, et al. Machine Learning in Polymer Informatics. InfoMat. 2021;3:353–61. doi: 10.1002/inf2.12167.
(80) Gude M, Müller-Pabel M, Koschichow R, Liebsch A. Morphological analysis and numerical modelling of the mechanical behaviour of polypropylene bead foams. Int J Mech Mater Des. 2017;7:569–74.
(81) Bürkle E, Schwachulla T. *Kunststoffe*. p. 21–8. https://www.kunststoffe.de/a/fachartikel/schaumperlen-im-aufwind-259698 (2019, accessed on 14 August 2023).
(82) Gude M, Stegelmann M, Müller M, Koschichow R, Liebsch A. Prüfmethodik Und Morphologiebasierte Simulation Des Strukturverhaltens Zur Auslegung von Partikelschäumen. In Particle Foam 2018, VDI Verlag; 2018. p. 131–40.
(83) Albuquerque RQ, Brütting C, Standau T, Ruckdäschel H. A machine learning investigation of low-density polylactide batch foams. e-Polymers. 2022;22:318–31. doi: 10.1515/epoly-2022-0031.
(84) Gebraad M, Kuijstermans FP, Noordegraaf J. Particulate, Expandable Polymer, a Method for Preparing the Same as Well as the Use Thereof. US Patent 8,901,181 B2; 2014.
(85) Miyagawa T, Hirose F, Senda K. Polyhydroxyalkanoate-based resin foamed particle, molded article comprising the same and proecss for producing the same 2011. US Patent 8,076,381 B2.
(86) Ocean Release: https://www.arpro.com/en-gb/news/news-2020/ocean-release/(accessed on 13 February 2023).
(87) ARPRO Revolution: https://www.arpro.com/en-GB/news/news-2020/arpro-revolution/(accessed on 13 February 2023).
(88) Tatzel H. Grundlagen der Verarbeitung von EPP – Bewährte und neue Verfahren. Thermoplastische Partikelschaumstoffe. Düsseldorf: VDI-Verlag GmbH; 1993.